Photoreactivity of ZnO nanoparticles in visible light: Effect of surface states on electron transfer reaction

Sunandan Baruah,[1] Sudarson Sekhar Sinha,[2] Barnali Ghosh,[2] Samir Kumar Pal,[2] A. K. Raychaudhuri,[2] and Joydeep Dutta[1,a)]

[1]*Center of Excellence in Nanotechnology, School of Engineering and Technology, Asian Institute of Technology, Klong Luang, Pathumthani 12120, Thailand*
[2]*Unit for Nano Science and Technology, S.N. Bose National Centre for Basic Sciences, JD Block, Sector III, Salt Lake, Kolkata 700 098, India*

Wide band gap metal oxide semiconductors such as zinc oxide (ZnO) show visible band photolysis that has been employed, among others, to degrade harmful organic contaminants into harmless mineral acids. Metal oxides show enhanced photocatalytic activity with the increase in electronic defects in the crystallites. By introducing defects into the crystal lattice of ZnO nanoparticles, we observe a redshift in the optical absorption shifting from the ultraviolet region to the visible region (400–700 nm), which is due to the creation of intermediate defect states that inhibit the electron hole recombination process. The defects were introduced by fast nucleation and growth of the nanoparticles by rapid heating using microwave irradiation and subsequent quenching during the precipitation reaction. To elucidate the nature of the photodegradation process, picosecond resolved time correlated single photon count (TCSPC) spectroscopy was carried out to record the electronic transitions resulting from the de-excitation of the electrons to their stable states. Photodegradation and TCSPC studies showed that defect engineered ZnO nanoparticles obtained through fast crystallization during growth lead to a faster initial degradation rate of methylene blue as compared to the conventionally synthesized nanoparticles. © *2009 American Institute of Physics*. [DOI: 10.1063/1.3100221]

I. INTRODUCTION

Toxic effluents from industries are a matter of serious concern for the environment, and much attention has been drawn toward the removal of harmful contaminants from waste water. Wide band gap metal oxide semiconductors are attractive candidates for the removal of pollutants in water as they are capable of acting as catalysts upon exposure to light radiation to degrade the harmful organic contaminants into harmless mineral acids. Photocatalysis has been established as an efficient process for the mineralization of toxic organic compounds,[1] hazardous inorganic materials,[2] and microbial disinfection[3] in water as a result of the formation of hydroxyl radical (OH·), which acts as a strong oxidizing agent.[4] Some of the commonly used metal oxide semiconductor photocatalysts are titanium dioxide (TiO_2), zinc oxide (ZnO), tungsten oxide (WO_3), strontium titanate ($SrTiO_3$), and hematite (α-Fe_2O_3).[5] Most of these semiconductor photocatalysts, except hematite, have a band gap in the ultraviolet (UV) region, i.e., equivalent to or larger than 3.2 eV (λ=387 nm), and promote photocatalysis upon illumination with UV radiation. The limited amount of UV light in the sun's spectra (around 7%) stands as a big obstacle in the direct use of solar energy for photocatalytic decomposition of organic and inorganic contaminants.

Photocatalysis using titania received much attention after the successful photolysis of water using TiO_2 photoanode upon irradiation with UV light with wavelength smaller than 190 nm in 1972.[6] The widely used titania nanoparticles (Degussa P25) in an aqueous colloidal dispersion show optical absorption peaking at around 220 nm with near zero absorption after 370 nm.[7] The reaction photoefficiency of the titania nanoparticles is very low,[8] which has been attributed to the scattering of light by the TiO_2 particles.[9] However, TiO_2 is not very active as a visible light photocatalyst. Visible light photocatalysis is activated in metal oxide semiconductors such as TiO_2 and ZnO through the presence of the inherent defect states in the nanocrystallites. Defect states can be created intentionally within the band gap through doping with transition metals.

With a large number of active sites, ZnO exhibits very high surface reactivity, rendering it an efficient visible light photocatalyst as compared to TiO_2. High reaction and mineralization rates[10] in ZnO photocatalysis have been reported due to the efficient generation of hydroxyl.[11] Surface and core defects in nanoparticles play a vital role in photocatalysis reactions. In ZnO, there is a multiplicity of levels, some deriving from residual impurities, some from oxygen deficiency, and others related to topographical irregularities.[12] Doping of ZnO nanoparticles can increase the photocatalytic activity as doping with metal and transition metals increases the surface defects,[13] thereby affecting the optical and electronic transitions.[14] There are reports of the enhancement of optical absorption in ZnO by doping with transition metal ions such as Ag, Pb, Mn, and Co.[13–16] Here, we report an increase in the visible light photolytic activity of ZnO by creating intentional defects in its crystal lattice through fast precipitation under microwave irradiation.

a)Electronic mail: joy@ait.asia.

105, 074308-1

We have systematically studied the photolytic activity of ZnO nanoparticles using controlled degradation of methylene blue (MB) using visible light from a tungsten halogen source closely resembling the solar spectra following the degradation process through single photon counting spectroscopy. The photolytic behavior of ZnO is correlated with the surface states that affect the electronic transitions upon exposure to photonic irradiation. To the best of our knowledge, there are no reports on the use of picosecond resolved time correlated single photon spectroscopy to explain the mechanism of the photoreaction of ZnO nanoparticles to date.

II. EXPERIMENTAL

Materials used: zinc acetate dihydrate $[(CH_3COO)_2Zn, 2H_2O]$, Merck; sodium hydroxide [NaOH], Merck; ethanol $[C_2H_5OH]$, J.T. Baker; methanol $[CH_3OH]$, Merck; isopropanol $[(CH_3)_2CHOH]$, Laboratory Scan; polyvinyl alcohol (PVA); and MB $[C_{16}H_{18}N_3CIS \cdot 3H_2O]$, Carlo Erba.

ZnO nanoparticle colloids were synthesized in ethanol following our earlier reports.[17,18] Briefly, a 4 mM zinc acetate solution and a 4 mM NaOH solution were prepared, both in ethanol under rigorous stirring at 50 °C. 20 ml of zinc acetate solution was complexed with 20 ml of pure ethanol, and the solution was heated at 70 °C for half an hour. 20 ml of the NaOH solution was then added to the mixture solution that was hydrolyzed for 3 h at 60 °C.

Fast crystallization and quenching of ZnO nanocrystallites during the precipitation reaction were carried out using a commercial microwave oven operated at the defrost mode. The defrost mode alternately switches between full power (800 W) and no power. The temperature of the zinc acetate solution in ethanol was adjusted to reach 65 °C after 5 min of microwave irradiation. After microwave excitation of the sample, ethanolic NaOH was added, and the solution was allowed to cool down to room temperature. Surface passivation was carried out by adsorbing 0.1% PVA prior to the addition of NaOH.

MB was used as the test contaminant for the photolysis experiments. A 10 μM sample of MB was prepared in ethanol and transferred to quartz cuvettes mixed with known quantities of ZnO nanoparticles. The cuvettes were then placed above a tungsten halogen light source (12 V and 55 W) for photodegradation. The intensity of light at the sample position was noted to be approximately 10 klux. Optical absorption spectra in the UV-vis region were recorded after every 30 s to follow the degradation of the organic dye. The steady state absorption and luminescence of the sample in the dark condition were measured using Shimadzu UV-vis and Fluoromax3 spectrophotometers, respectively. Time correlated single photon count spectroscopy [Edinburgh Instruments Life Spec-PS, instrument response function (IRF) 73 ps] was used to measure the lifetime of the excited electrons of the ZnO nanoparticles.

X-ray diffraction (XRD) was measured to record the (θ-2θ) diffraction of lyophilized (Thermo) ZnO powder using an X-pert Pro machine (Philips Panalytical) with Cu $K\alpha$ radiation. Phase formation and phase purity were confirmed
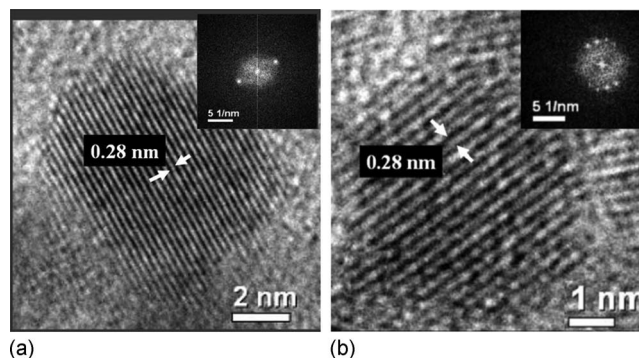

FIG. 1. (a) High resolution transmission electron microscopy (HRTEM) image of the ZnO nanoparticle (conventional). Inset: SAED pattern (b) HRTEM image of the ZnO nanoparticle (microwave). Inset: SAED pattern.

by XRD data. The XRD data were used to estimate the average particle size (using the Williamson Hall plot). Transmission electron microscopy (TEM) was performed using a JEOL JEM 2010 operating at 120 kV. Samples for TEM were prepared by using sonicated dilute colloids on carbon coated TEM grids followed by controlled drying prior to the microscopy.

III. RESULTS AND DISCUSSION

The ZnO nanoparticles synthesized by hydrolysis over a period of 3 h (conventional method) and the ones synthesized using microwave irradiation (microwave method) yielded nanoparticles that were spherical and highly monocrystalline, as shown in Fig. 1. The average particle size estimated from XRD data agreed with that obtained from the TEM ($\sim$5–7 nm).

Measurements done using image processing software (SCION IMAGE) show lattice fringe widths of 0.28 nm in both the cases indicating the (001) plane of the wurtzite structure of the ZnO crystal. The high crystallinity of the particles is evident from the selected area electron diffraction (SAED) pattern shown in the insets in Figs. 1(a) and 1(b). Figure 2 shows the optical absorption spectra of the nanoparticles. The particles synthesized using the microwave method shows higher optical absorption in the visible region (400–700 nm) compared to the conventionally synthesized ZnO nanoparticles.
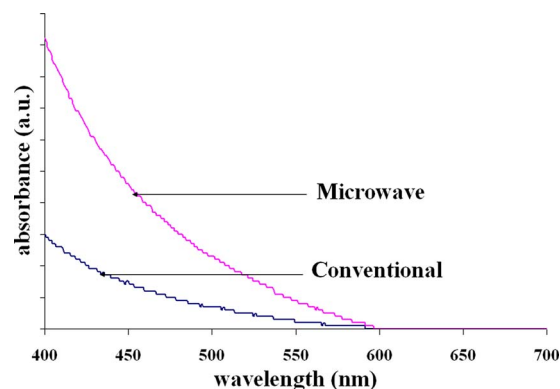

FIG. 2. (Color online) Optical absorption spectra of the ZnO nanoparticles in the visible range between 400 and 700 nm. Microwave synthesized particles are better visible light absorbers.
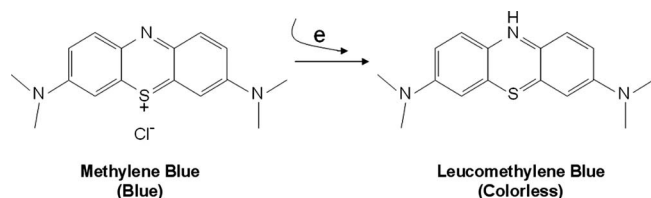
FIG. 3. Schematic diagram showing the conversion of MB into LMB with the addition of an electron.

MB is electroactive and is capable of accepting electrons. It accepts electrons and degrades into leucomethylene blue (LMB), which is colorless,[19] as shown schematically in Fig. 3. The photodegradation of MB (blue in color) to LMB (colorless) was observed by monitoring the MB peak absorption (655 nm) upon continued light exposure.

The degradation of MB in the presence of conventionally synthesized nanoparticles followed an almost exponential decay (Fig. 4), with the rate of degradation gradually decreasing with time. The microwave synthesized nanoparticles induce a much faster initial degradation as compared to the conventional nanoparticles (Fig. 4, inset). Upon deconvolution of the decay curves, as shown in Fig. 4, a much faster decay component was observed for the degradation using microwave synthesized nanoparticles ($\tau_1 = 140$ s) compared to the conventional ones ($\tau_1 = 280$ s). This indicates the presence of more active sites for the transfer of electrons in the microwave synthesized nanoparticles (which are of the same size as conventional particles), which may be due to inherent defects or electron vacancies in the crystal lattice as a result of faster nucleation and growth. In order to understand the nature of the photodegradation process of MB in the presence of ZnO nanoparticles, concentration (dye) dependent kinetics experiments were carried out. From the experimental results, we have observed that for the lower relative concentration of MB compared to ZnO nanoparticles (ZnO:MB=5:1), the rate of degradation depends on the concentration of MB in the dispersion. However, upon increasing the MB concentration higher than that of the ZnO nanoparticles, the kinetics rate becomes independent of the concentration of MB.

It is to be noted that any kind of surface catalyzed reaction is expected to follow the Langmuir–Hinshelwood model,[20] where the rate of reaction depends on the concentration of the reactants in the dispersion. In a review on photocatalytic degradation of azo dyes containing different functionalities using TiO_2 as a photocatalyst in aqueous dispersion under solar and UV irradiation, Konstantinou and Albanis[20] noted that the mechanism of the photodegradation depends on the radiation used. Charge separation occurred under UV light radiation and charge injection from the semiconductor to the dye under visible radiation. Kinetics analyses indicated that the photodegradation rates of azo dyes can be approximated as first-order kinetics in accordance with the Langmuir–Hinshelwood model. Lakshmi *et al.*[21] observed that the oxidation of MB through titania assisted photocatalysis conforms to a Langmuir adsorption isotherm. In a similar report, Zhang *et al.*[22] opined that the kinetics of photodegradation of MB in titania dispersions follows the Langmuir–Hinshelwood model as they noticed a change in the kinetics with the initial concentration of MB. The surface attachment and detachment of the reactant in the active site are also crucial for the surface reaction. From our observation, it is revealed that the photodegradation reaction of MB in the presence of ZnO nanoparticles is not of Langmuir–Hinshelwood type. Here we conclude that the photoproduct, LMB, is not detached from the ZnO surface. Thus for higher concentrations of MB, the reaction rate is independent of the change in the concentration of MB. Our observations clearly indicate that the photodegradation of MB is not catalyzed by the ZnO nanoparticles. A similar observation using titanium dioxide has been reported by Emeline *et al.*[23] recently.

In an attempt to comprehend the photolytic process, which is known to take place due to electronic transitions between the ZnO nanoparticles and MB molecules, picosecond resolved time correlated single photon count spectroscopy was carried out to observe the electronic activity in the ZnO nanoparticles, both in the presence and the absence of MB. It has to be noted that our interest is to understand the photolysis of a model organic molecule (MB) by a ZnO nanoparticle in the presence of solar radiation. Thus in the present study, we have used excitation light of 375 nm, which is abundant in the solar spectrum, instead of deep UV light, responsible for band edge transition. The temporal decay of luminescence intensity measured using picosecond spectroscopy with the ZnO nanoparticle samples revealed an excited state lifetime, which is multiexponential (Fig. 5) and is of the form

$$I(t) = A + \sum_{i=1}^{4} B_i \exp\left(\frac{-t}{\tau_i}\right), \tag{1}$$

where A is the base line factor and B_i's are the preexponential factors. The lifetime values (τ_i) of the systems can be attributed to the transitions from the excitation band to the valence band and/or the coupled defect states. The slower component can be reasoned to arise from the elec-
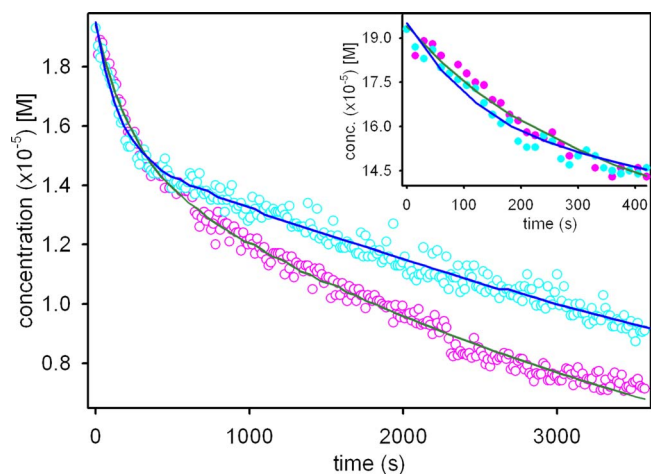

FIG. 4. (Color online) Decrease in concentration of MB at 655 nm in the presence of the conventional and microwave synthesized ZnO nanoparticles upon exposure to light from a tungsten halogen source (10 klux) as a function of time. Inset: initial faster degradation observed in the case of microwave synthesized nanoparticles.
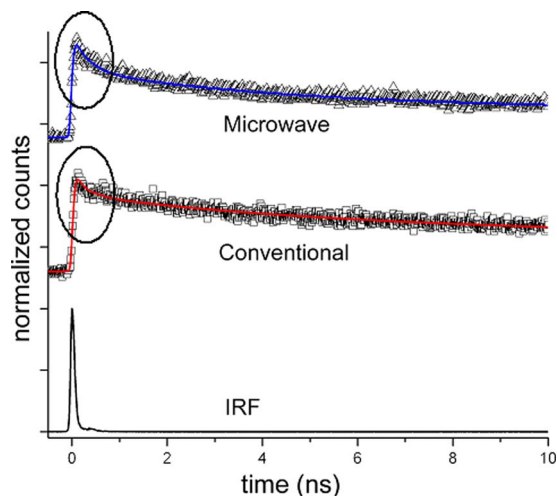
FIG. 5. (Color online) Fluorescence transients observed at 560 nm for conventional and 570 nm for microwave synthesized ZnO nanoparticles. The Instrument Response Function (IRF) was about 70 ps [full width at half maximum (FWHM)]. The faster decay part is highlighted.

FIG. 7. (Color online) Fluorescence transients observed at 560 nm for conventional ZnO nanoparticles: (1) ZnO and MB after 3 h exposure to visible light. (2) After adding excess MB to (1). (3) (2) After 3 h exposure to visible light. The faster decay part is highlighted.

trons transiting from defect or electron deficient states to recombine with holes in the valence band.

The electrons move to the defect states from the edge of the conduction band through nonradiative (phononic) transitions. The various decay time periods of the excited electrons calculated from the photoluminescence spectral decay at the wavelengths of 560 and 570 nm are given in Tables I and II, respectively. The average lifetime is calculated using the following equation:

$$\langle \tau_{av} \rangle = \sum_{i=1}^{n} B_i \tau_i = \frac{1}{(k_r + k_{nr})},$$ (2)

where k_r and k_{nr} are the radiative and nonradiative rate constants of the electronic transitions, respectively. In the case of pure ZnO in ethanol (Fig. 6), the state lifetime ($k_{nr}=0$) of conventionally synthesized ZnO nanoparticles is 26.8 ns, which is comparable to the microwave synthesized nanopar-

ticles (25.2 ns), which gives the radiative rate constants of 3.73×10^7 and 3.96×10^7 s^{-1}, respectively. Upon the addition of MB to the nanoparticles, the average lifetimes were found to reduce to 6.84 and 4.07 ns, which give the rate constants of 14.6×10^7 and 24.6×10^7 s^{-1}, respectively. Using Eq. (2), we have calculated the electron transfer rate, which is directly reflected in the nonradiative rate constant (k_{nr}). The calculated nonradiative rate constants are 1.08×10^8 and 2.06×10^8 s^{-1} for the conventional and the microwave ZnO nanoparticles, respectively. From the above k_{nr} values, we can conclude that the microwave synthesized nanoparticles are much more effective toward the photooxidation in the presence of the model organic pollutant, MB.

We have observed that k_{nr} decreases significantly after 3 h of incubation of ZnO with MB in the presence of visible light (Fig. 7). In order to clarify whether the decrease in activity with time is a result of immobilized photoproduct
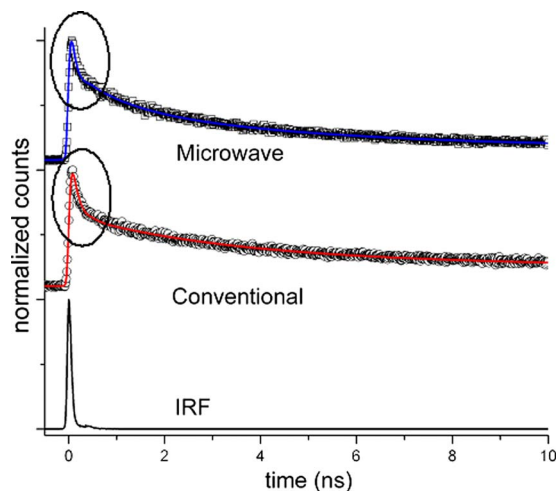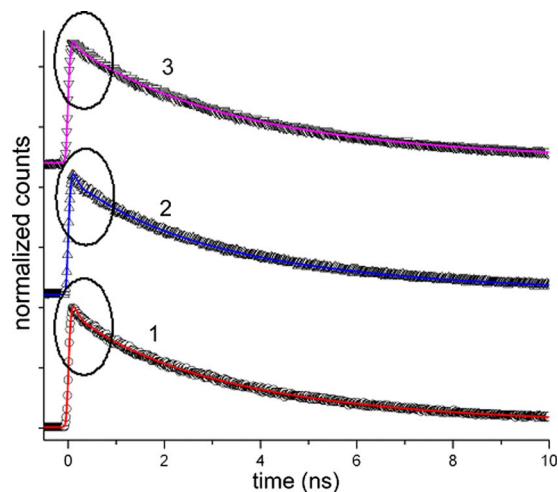

FIG. 6. (Color online) Fluorescence transients observed at 560 nm for conventional and 570 nm for microwave synthesized ZnO nanoparticles in the presence of MB. The IRF was about 70 ps (FWHM). The faster decay part is highlighted.
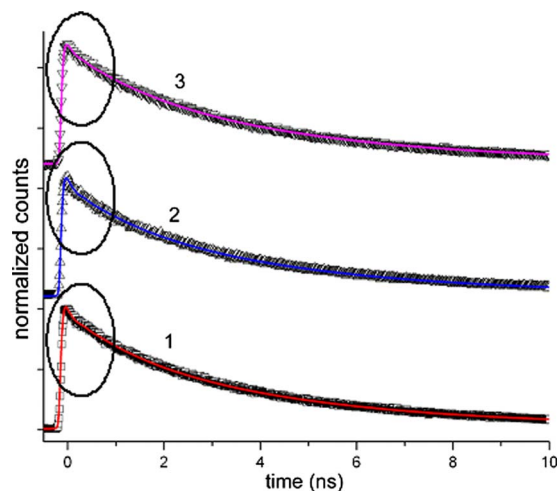

FIG. 8. (Color online) Fluorescence transients observed at 570 nm for microwave ZnO nanoparticles: (1) ZnO and MB after 3 h exposure to visible light. (2) After adding excess MB to (1). (3) (2) After 3 h exposure to visible light. The faster decay part is highlighted.

TABLE I. Picosecond decay periods of luminescence measured with ZnO nanoparticles (bare or with MB) synthesized by the conventional method. 1, ZnO nanoparticles only; 2, ZnO+MB; 3, 2 after 3 h exposure to 10 klux visible light; 4, 3+MB; 5, 4 after 3 h further exposure to 10 klux visible light (figures in parens indicate percentage population of excited electrons).

	1	2	3	4	5
τ_1	0.139 ns (16.0%)	0.125 ns (62.1%)	0.151 ns (31.5%)	0.123 ns (30.2%)	0.147 ns (27.4%)
τ_2	1.19 ns (8.0%)	3.24 ns (23.5%)	1.77 ns (18.5%)	1.47 ns (17.4%)	1.89 ns (18.5%)
τ_3	5.2 ns (16.0%)	⋯	4.34 ns (48.6%)	4.24 ns (51.6%)	4.53 ns (53.4%)
τ_4	43.1 ns (60.0%)	41.74 ns (14.4%)	37.11 ns (1.4%)	33.36 ns (1.3%)	30.14 ns (0.7%)

target molecules (LMB) adsorbed onto the surface of the nanoparticles, spectroscopic study was carried out after degrading the MB for 3 h under visible light illumination followed by addition of excess MB. The various decay time constants obtained after deconvolution of the decay curves with IRF (Figs. 7 and 8) are given in columns 3–5 in Tables I and II.

The fraction of the electrons following the faster decay path decreased sharply from 62.1% to about 30% in both the cases of conventional as well as microwave synthesized nanoparticles, validating the presumption that the photoproduct of MB molecules (LMB) were getting immobilized on the ZnO surface. The very low population of electrons in the slow decay path may result from passivation of surface defects due to the surface mediated LMB molecules from adsorbed MB. It is to be noted that the kinetics rates of the MB degradation (33.3×10^7 s^{-1} with conventional ZnO nanoparticles and 35.9×10^7 s^{-1} for microwave synthesized ZnO nanoparticles) remain almost unaltered upon further addition of MB after 3 h of degradation of the same sample, reconfirming the inability of unreduced MB molecules to be adsorbed further on the ZnO nanoparticle surfaces.

In order to further confirm that surface passivated ZnO nanoparticles are not active for the photodegradation, kinetics studies were performed using the ZnO nanoparticles passivated with PVA. Incubation of MB with PVA-capped ZnO nanoparticles in the presence of the radiation from the tungsten halogen light showed insignificant photodeterioration of MB molecules; the kinetics rate of the PVA-capped system is 36.9×10^7 s^{-1}, which is similar to the kinetics rate observed for the readsorbed MB on ZnO nanoparticles after initial degradation. The picosecond resolved photoluminescence decay constants are shown in Table III. The complete disappearance of the slower decay component (τ_4) compared to those observed in the ZnO nanoparticles without MB suggests that τ_4 arises due to surface defects. The passivated

defects also minimize the possibility of coupling between the bulk and the surface states, which explains the change in the faster component (τ_1) from 0.14 ns in the ZnO conventional and microwave nanoparticles (Tables I and II) to 1.19 and 0.34 ns, respectively, after passivation with PVA (Table III).

The process of photodegradation using the ZnO nanoparticles as a consequence of electron transfer from the surface of the nanoparticles is represented in a schematic model shown in Fig. 9. Upon excitation with a photon of sufficient energy, electron hole pairs are created, and the electrons may jump up to the conduction band or to defect states close to the conduction band. The separated electrons are capable of reducing an acceptor molecule (A) adsorbed on its surface, and holes can oxidize donor molecules (D). Electron hole pair recombination takes place after the optically excited electrons lose energy through radiative and nonradiative paths and fall back to the valence band. Optical excitations to conduction band edge (350 nm and 3.54 eV) and one of the defect bands (375 nm and 3.31 eV) are shown by curved arrows (Fig. 9). Using a similar model, the origin of two photoluminescence lines from singly and doubly charged oxygen vacancy centers in ZnO nanoparticles at 497 and 565 nm, respectively, has been proposed.[24] Visible emission in ZnO has also been attributed to oxygen vacancies.[25] A depletion layer exists in proximity to the surface of the spherical nanoparticles, the thickness of which is determined by the density of native carrier concentration in the nanoparticles. The Fermi level in the colloidal ZnO nanoparticles is typically higher than the solvent (ethanol in this case) in which it is suspended[26] and the MB molecules adsorbed onto its surface. The photoluminescence spectra of conventional ZnO and microwave ZnO nanoparticles revealed emissions peaking at 560 and 570 nm, respectively, when excited with an optical source at 375 nm. This green emission may be accredited to radiative decay from doubly charged oxygen vacancies.[24,25] The adsorbed MB molecules on ZnO nanopar-

TABLE II. Picosecond decay periods of luminescence measured with ZnO nanoparticles (bare or with MB) synthesized by the microwave method. 1, ZnO nanoparticles only; 2, ZnO+MB; 3, 2 after 3 h exposure to 10 klux visible light; 4, 3+MB; 5, 4 after 3 h further exposure to 10 klux visible light (figures in brackets indicate percentage population of excited electrons).

	1	2	3	4	5
τ_1	0.137 ns (28.1%)	0.078 ns (62.1%)	0.125 ns (29.6%)	0.141 ns (32.4%)	0.156 ns (26.9%)
τ_2	1.24 ns (12.3%)	0.86 ns (13.8%)	1.26 ns (17.8%)	1.41 ns (17.6%)	1.59 ns (18.4%)
τ_3	7.06 ns (14.0%)	3.86 ns (19.1%)	4.16 ns (51.3%)	4.25 ns (49.3%)	4.33 ns (53.9%)
τ_4	52.68 ns (45.6%)	45.38 ns (7.44%)	29.87 ns (1.3%)	38.86 ns (0.7%)	27.3 ns (0.7%)

TABLE III. Picosecond decay periods in ZnO nanoparticle colloid surface passivated with PVA (figures in brackets indicate percentage population of excited electrons).

	τ_1	τ_2	τ_3
Conventional	1.19 ns (26.53%)	3.185 ns (72.79%)	10.85 ns (0.68%)
Microwave	0.399 ns (48.13%)	2.392 ns (40.63%)	4.776 ns (11.25%)

ticles are reduced through faster electron transfer mechanisms as compared to recombination processes from the excited species. The surface defects in ZnO nanoparticles lead to a band bending in the tail states (Fig. 9) that contributes to the reduction in the MB upon adsorption onto ZnO. LMB formed by the injection of electrons into the adsorbed MB on the nanoparticles blocks the possibility of further electron transfer from the nanoparticles. Desorption of the LMB would be necessary for subsequent photolytic reduction in MB.

IV. CONCLUSION

ZnO nanoparticles were successfully synthesized through controlled hydrolysis as well as through microwave induced nucleation and growth. Photolytic degradation tests carried out on a test contaminant MB revealed faster initial degradation with ZnO nanoparticles synthesized using microwave irradiation for introducing electronic defects. Time correlated single photon count spectroscopic studies were conducted to explain the photoreactivity of ZnO nanoparticles in terms of electronic transitions between nanoparticles and the target MB molecules. Spectroscopic studies upon surface passivation of defects on ZnO nanoparticles with PVA confirm that photolysis reactions are controlled by inherent defects on the ZnO surface. The basic aim of our work is to investigate the role of electron transfer dynamics from ZnO nanoparticles to MB during the photodegradation of MB at the nanoparticle surface. Our studies suggest that for successful and repeated photocatalysis of MB on ZnO nanoparticles, desorption of the by-product, LMB will be necessary. Further work is in progress to elucidate this.
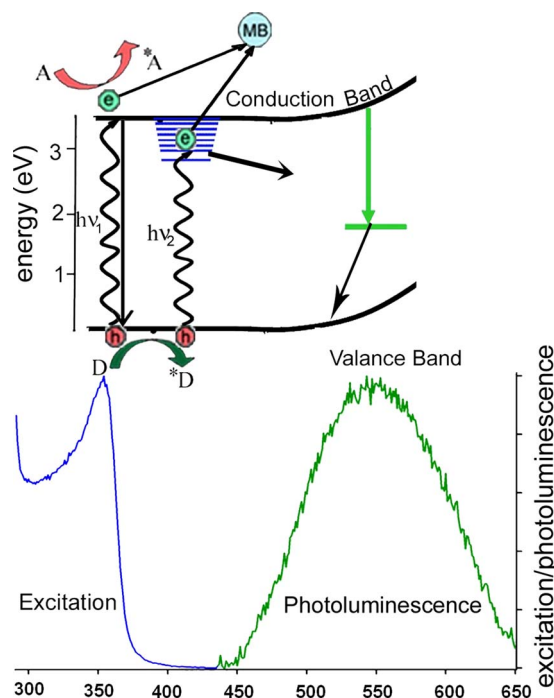
FIG. 9. (Color online) Schematic diagram showing the possible electronic transitions upon excitation with a photon. D and *D represent donor molecules before and after oxidation. A and *A represent acceptor molecules before and after they are reduced. Electron hole pair recombination takes place after the optically excited electrons lose energy through radiative and nonradiative paths and fall back to the valence band. Optical excitations to conduction band edge (350 nm and 3.54 eV) and one of the defect bands (375 nm and 3.31 eV) are shown by curved arrows. The lower panel shows the excitation applied on the ZnO nanoparticles and the corresponding green emission from doubly charged oxygen vacancies.

[1] K. Nakano, E. Obuchi, S. Takagi, R. Yamamoto, T. Tanizaki, M. Taketomi, K. Eguchi, K. Ichida, M. Suzuki, and A. Hashimoto, Sep. Purif. Technol. **34**, 67 (2004).
[2] J. M. Herrmann, Catal. Today **53**, 115 (1999).
[3] P. C. Maness, S. Smolinski, D. M. Blake, Z. Huang, E. J. Wolfrum, and W. A. Jacoby, Appl. Environ. Microbiol. **65**, 4094 (1999).
[4] Z. Huang, P. C. Maness, D. Blake, E. J. Wolfrum, S. L. Smolinski, and W. A. Jacoby, J. Photochem. Photobiol., A **130**, 163 (2000).
[5] D. S. Bhatkhande, D. S. Pangarkar, and A. A. Beenackers, J. Chem. Technol. Biotechnol. **77**, 102 (2001).
[6] A. Fujishima and K. Honda, Nature (London) **238**, 37 (1972).
[7] I. N. Martyanov, E. N. Savinov, and K. J. Klabunde, J. Colloid Interface Sci. **267**, 111 (2003).
[8] E. Wilson, Chem. Eng. News **1**, 29 (1996).
[9] M. I. Cabrera, O. M. Alfano, and A. E. Cassano, J. Phys. Chem. **100**, 20043 (1996).
[10] I. Poulios, D. Makri, and X. Prohaska, GlobalNest: The Int. J. **1**, 55 (1999).
[11] E. R. Carraway, A. J. Hoffman, and M. Hoffman, Environ. Sci. Technol. **28**, 786 (1994).
[12] T. J. Gray and P. Amigues, Surf. Sci. **13**, 209 (1969).
[13] R. Wang, J. H. Xin, Y. Yang, H. Liu, L. Xu, and J. Hu, Appl. Surf. Sci. **227**, 312 (2004).
[14] K. Vanheusden, W. L. Warren, J. A. Voigt, C. H. Seager, and D. R. Tallant, Appl. Phys. Lett. **67**, 1280 (1995).
[15] R. Ullah and J. Dutta, J. Hazard. Mater. **156**, 194 (2008).
[16] S. Colis, H. Bieber, S. B. Colin, G. Schmerber, C. Leuvrey, and A. Dinia, Chem. Phys. Lett. **422**, 529 (2006).
[17] M. K. Hossain, S. C. Ghosh, Y. Boontongkong, C. Thanachayanont, and J. Dutta, J. Metastable Nanocryst. Mater. **23**, 27 (2005).
[18] A. Sugunan, H. C. Warad, M. Boman, and J. Dutta, J. Sol-Gel Sci. Technol. **39**, 49 (2006).
[19] See: www.udel.edu/pchem/C446/Experiments/exp7.pdf
[20] I. Konstantinou and T. Albanis, Appl. Catal., B **49**, 1 (2004).
[21] S. Lakshmi, R. Renganathan, and S. Fujita, J. Photochem. Photobiol., A **88**, 163 (1995).
[22] T. Zhang, T. Oyama, A. Aoshima, H. Hidaka, J. Zhao, and N. Serpone, J. Photochem. Photobiol., A **140**, 163 (2001).
[23] A. V. Emeline, V. K. Ryabchuk, and N. Serpone, Catal. Today **122**, 91 (2007).
[24] M. Ghosh and A. K. Raychaudhuri, Nanotechnology **19**, 445704 (2008).
[25] A. van Dijken, E. Meulenkamp, D. Vanmaekelbergh, and A. Meizerink, J. Lumin. **87-89**, 454 (2000).
[26] F. Qu and P. C. Morais, J. Chem. Phys. **111**, 8588 (1999).